Published in final edited form as:
Biochemistry. 2005 June 21; 44(24): 8817–8825. doi:10.1021/bi047400+.

Influence of the 33 kDa Manganese-Stabilizing Protein on the Structure and Substrate Accessibility of the Oxygen-Evolving Complex of Photosystem II†

Wolfgang Gregor[*,‡,§], **Roehl M. Cinco**[‖], **Hui Yu**[‡], **Vittal K. Yachandra**[‖], and **R. David Britt**[‡]
Department of Chemistry, University of California, Davis, California 95616, and Melvin Calvin Laboratory, Physical Biosciences Division, Lawrence Berkeley National Laboratory, Berkeley, California 94720-5230

Abstract

The 33 kDa manganese-stabilizing extrinsic protein binds to the lumenal side of photosystem II (PS II) close to the Mn_4Ca cluster of the oxygen-evolving complex, where it limits access of small molecules to the metal site. Our previous finding that the removal of this protein did not alter the magnetic coupling regime within the manganese cluster, measured by electron spin-echo envelope modulation [Gregor, W., and Britt, R. D. (2000) *Photosynth. Res. 65*, 175–185], prompted us to examine whether this accessibility control is also true for substrate water, using the same pulsed EPR technique. Comparing the deuteron modulation of the S_2-state multiline signal of PS II membranes, equilibrated with deuterated water (D_2O) after removal or retention of the 33 kDa protein, we observed no change in the number and the distance of deuterons magnetically coupled to manganese, indicating that the number and distance of water molecules bound to the manganese cluster are independent of bound 33 kDa protein in the S_1 state, in which the sample was poised prior to cryogenic illumination. A simple modulation depth analysis revealed a distance of 2.5–2.6 Å between the closest deuteron and manganese. These results are in agreement with our refined X-ray absorption analysis. The manganese K-edge positions, reflecting their oxidation states, and the extended X-ray absorption fine structure amplitudes and distances between the manganese ions and their oxygen and nitrogen ligands (1.8, 2.7, and 3.3–3.4 Å) were independent of bound 33 kDa protein.

Oxidation of ubiquitous water to dioxygen is the basis for plant-type (oxygenic) photosynthesis, carried out by cyanobacteria, algae, and green plants. It produces the majority of the earth's biomass, and the resultant dioxygen delivered into the atmosphere

†This work was funded by National Institutes of Health Grants GM48242 (R.D.B.) and GM55302 (V.K.Y.), the Director, Office of Science, Office of Basic Energy Sciences, Chemical Sciences, Geo-sciences, and Biosciences Division of the Department of Energy, under Contract DE-AC03-76SF00098 (V.K.Y.), and the Ford Foundation (predoctoral fellowship, R.M.C.). Synchrotron radiation facilities were provided by the Stanford Synchrotron Radiation Laboratory (SSRL), which is operated by the Department of Energy, Office of Basic Energy Sciences. The SSRL Biotechnology Program is supported by the National Institutes of Health, National Center of Research Resources, Biomedical Technology Program, and by the Department of Energy, Office of Health and Environmental Research.

[*]To whom correspondence should be addressed. Phone: +43-1-25077-4419. Fax: +43-1-25077-4490. Wolfgang.Gregor@vu-wien.ac.at.
[‡]University of California, Davis.
[§]Present address: Research Institute of Biochemical Pharmacology and Toxicology, University of Veterinary Medicine Vienna, Vienna, Austria.
[‖] Lawrence Berkeley National Laboratory.

Supporting Information **Available**: Results of the EXAFS analysis (Table 1) and a description of the fitting methodology. This material is available free of charge via the Internet at http://pubs.acs.org.

allows for aerobic life. This water-splitting reaction, in essence the reversal of respiratory dioxygen consumption, is catalyzed by the oxygen-evolving complex (OEC[1]) of photosystem II (PS II). PS II is a transmembrane protein complex of the thylakoid membrane which is located in the chloroplast in algae and plants (1). PS II consists of ca. 25 different polypeptide subunits and is organized as a core structure with ca. 20 subunits, surrounded by the chlorophyll-containing light-harvesting complex which functions as an antenna. The catalytic heart of the core is the reaction center formed by the D1 and D2 proteins which bind the redox cofactors constituting the electron transport chain from the light-excited primary donor P_{680} (a chlorophyll *a* species) to plastoquinone Q_B, with pheophytin and plastoquinone Q_A intermediates. The highly oxidizing radical P_{680}^+ is ultimately rereduced by water. The coupling of the four-electron oxidation of two water molecules (yielding one dioxygen molecule) to the one-electron chemistry of P_{680} necessitates a well-regulated catalytic unit acting as a charge accumulator, to prevent formation of partially oxidized water-derived species such as superoxide and peroxide which would be cytotoxic upon premature release from the protein. This is all accomplished by the OEC, localized at the lumenal side of the PS II reaction center (2, 3).

It is widely accepted that the OEC consists of a tetramanganese cluster, additional essential cofactors (one Ca^{2+} ion and one Cl^- ion), and a redox-active tyrosine of the D1 protein, Y_Z. From EXAFS studies, the structure was shown to include two or three 2.7 Å Mn–Mn distances and a Mn–Mn distance at 3.3 Å, including one or two Mn–Ca distances at 3.4 Å. Several topological models were proposed on the basis of these parameters (3). More recently, one of the models, a trimer–monomer or “dangler” model, was shown to give a good interpretation of EPR and ENDOR data (4). The two first crystal structures of oxygen-evolving PS II at 3.8 Å (5) and 3.7 Å (6) resolution were inconclusive as to the exact arrangement of the Mn ions, whereas the most recent crystal structure proposed a cubelike Mn_3CaO_4 cluster connected to a fourth Mn ion bridged via a single oxygen at the corner of the cube (7). In this model, the amino acid residues which serve as Mn ligands—at least one histidine, two aspartate, and two glutamate residues—are provided by the D1 protein, and another glutamate is provided by the CP43 protein.

Despite intensive biophysical research, the mechanism by which the OEC splits water is still unknown. The framework for the mechanism of water oxidation is provided by the Kok cycle model (8): four successive photooxidation steps of P_{680} drive four successive one-electron oxidation steps of the OEC (the S-state transitions), with tyrosine Y_Z mediating electron transfer between the OEC and P_{680}. Once the cluster is assembled and undergoing active turnover, the most reduced functional state is termed S_0, and following four sequential photooxidation steps, the resulting transient S_4 state releases product O_2 and the OEC is cycled back to the S_0 state. The S_1 state is the dark stable state and lacks EPR signals in the standard, perpendicular polarization mode, whereas the S_2 state is well-characterized by a spin $S = 1/2$ multiline EPR signal at $g = 2$ featuring ca. 18–22 ^{55}Mn hyperfine lines, in addition to a broad $g = 4.1$ signal which is attributed to a higher spin state of the Mn cluster (2, 9).

Various structural models of the OEC and mechanistic models of water oxidation have been proposed on the basis of structural insights from EXAFS and EPR spectra, XANES-derived oxidation states of the Mn ions, the chemistry of model Mn complexes, mass-spectrometry-derived H_2O exchange rates, H^+ release kinetics, EPR- and UV-spectroscopy-derived electron-transfer kinetics, and theoretical calculations (10–16). The most recent crystal

[1]Abbreviations: CW, continuous wave; ENDOR, electron nuclear double resonance; EPR, electron paramagnetic resonance; ESEEM, electron spin-echo envelope modulation; EXAFS, extended X-ray absorption fine structure; OEC, oxygen-evolving complex; PS II, photosystem II; XANES, X-ray absorption near edge structure; XAS, X-ray absorption spectroscopy.

structure of PS II (7) imposes further constraints (17). There is a large consensus that the Mn_4Ca cluster is the site of substrate water binding and oxidation, that at least three of four Kok transitions involve Mn oxidation, and that electron transfer to Y_Z is coupled to substrate-derived proton or hydrogen abstraction by $Y_Z^{\bullet}$ in one or more Kok cycle transitions. However, basic questions remain open. The following are examples: At which S-state transitions do the two substrate water molecules bind and at which steps are they oxidized? What is the specific nature of substrate binding? Are both substrate water molecules bound to Mn ions or might one be bound to the essential Ca cofactor?

EPR spectroscopy probing substrate, substrate analogue, and inhibitor binding, including the use of specific labeled isotopes, can directly address such questions. For example, the following results were obtained: (i) Line broadening of the multiline CW-EPR signal of PS II preparations equilibrated with $H_2{}^{17}O$ suggested water ligation to Mn (18). (ii) Complementing ESEEM experiments (vide infra) using the same type of samples revealed coupling between Mn and ^{17}O (19). (iii) Pulsed ENDOR of the S_2-state multiline signal, using untreated PS II or PS II equilibrated with D_2O, revealed exchangeable protons strongly coupled to Mn (15). (iv) Complementing ESEEM experiments using the same type of samples also revealed strong isotropic coupling to exchanged deuterons and allowed for a quantitative analysis: the best fit was obtained with three groups of two deuterons at 2.67, 2.71, and 3.43 Å, respectively, in a point dipolar approximation (15). This was considered compatible with substrate ligated to Mn in the S_1 and S_2 states. (v) ESEEM of the S_0-state multiline signal, also using the same type of samples, suggested substrate binding in the initial S_0 state (15). (vi) ESEEM of PS II treated with methanol deuterated at the nonexchangeable methyl hydrogens showed methanol binding near (or directly to) the Mn cluster in the S_1 and S_2 states (20), and ESEEM of PS II treated with ^{14}N or ^{15}N ammonia showed ammonia ligation to Mn in the S_2 state (21). ESEEM studies on PS II simultaneously treated with deuterated methanol and ammonia showed that both ligands bind independently (Evanchik, M. A., Peloquin, J. M., and Britt, R. D., unpublished results), and it is appealing to consider this evidence for two distinct substrate-binding sites at the OEC. (vii) The induction of the S_0-state multiline signal by methanol (22, 23) also suggested methanol binding in S_0, thus reflecting substrate binding in S_0 in the absence of the alcohol. These EPR-based results can be compared with those from time-resolved mass spectrometry probing S-state-dependent substrate exchange: Wydrzynski (12) found that two substrate molecules bind and probably react asymmetrically. The first H_2O molecule is already bound in the S_0 state, but the second does not bind before formation of the S_3 state.

Ordered substrate binding—both spatially (to achieve proper orientation for O—O bond formation) and temporally (in the course of the Kok cycle)—seems essential for optimal functioning of the OEC. At the same time, exclusion of potential exogenous reductants from the highly oxidizing OEC would be beneficial. Such an accessibility control has been ascribed to three extrinsic protein subunits of PS II which bind to its lumenal side (24), in particular the 33 kDa protein (named after its apparent molecular mass), also called the manganese-stabilizing protein (25); in its absence the OEC remains relatively stable and enzymatically active, demonstrating that this protein is not essential for creating a structurally intact and functioning OEC, and suggesting that the protein is not involved in Mn binding. No Mn ligands from the 33 kDa proteins are assigned in the crystal structure of PS II (7). However, for function without the 33 kDa protein, at least 100 mM Cl^- must be provided in the buffer medium; at low Cl^- concentration, two of the four Mn ions are released from their site and the activity is lost. Two additional proteins, with apparent molecular masses of 17 and 23 kDa, further stabilize the binding of the Cl^- as well as the Ca^{2+} cofactor at physiological concentrations of these ions (24).

One copy of each of these proteins binds to the PS II core. An 8 Å structure of plant PS II, based on single-particle electron microscopy, revealed the location of the 33 kDa protein and the 17/23 kDa proteins, which form lumenal side caps on the D2 and D1 proteins of the reaction center (26). The crystal structures of cyanobacterial PS II confirm this position of the 33 kDa protein, showing a 35–45 Å long β-cylinder tilted against the membrane by 45° and approaching the membrane interface close to the Mn site (5–7). In a previous ESEEM report (27) we showed that the structural integrity of the Mn cluster, including the histidine-derived N-ligand, is retained in the S_1 and S_2 states upon removal of all three extrinsic proteins under appropriate salt conditions (200 mM Cl^-, 10 mM Ca^{2+}), and in a previous EXAFS study (28) we failed to detect changes of the 1.8 Å Mn–O/N and 2.7 Å Mn–Mn vectors, providing a rationale for the observation that these proteins are not required for catalytic activity.

However, removal of the extrinsic proteins leads to some changes of reactivity of the OEC: the access of exogenous ligands or reductants of Mn is generally enhanced, and the absence of the 33 kDa protein slows the $S_3 \rightarrow (S_4) \rightarrow S_0$ transition (25). It has been proposed that the 33 kDa protein forms a water channel that allows controlled substrate access to the OEC, hence optimizing the overall water oxidation rate (29). The effect of the 33 kDa protein on OEC reactivity could be direct, or indirect via allosteric interactions with other subunits. Although it is concluded from the crystal structure (7) that the 33 kDa protein does not provide any of the Mn ligands, a direct interaction with the OEC, i.e., a participation in forming the OEC cleft within the PS II complex and thus a control of substrate binding, seems possible from its location close to the Mn site (vide supra). On the other hand, similar features of 33 kDa protein-depleted compared to Cl-depleted, 33 kDa protein-intact PS II samples were taken as evidence that the 33 kDa protein acts entirely by maintaining Cl^- in its functional site. As to indirect interactions, single-particle electron microscopy indeed detected specific long-range structural rearrangements of PS II (30): removal of the 17 and 23 kDa proteins or of all three extrinsic proteins resulted in a ca. 1 nm shift of the antenna protein CP29 or of the light-harvesting complex trimer, respectively, toward the PS II core. The presence of the 33 kDa protein also changes the conformation of the lumenal side of reaction center protein(s), probably D2, so that the 23 kDa protein binds more strongly to its docking site (24). In addition to the effects of the binding of the 33 kDa protein on the structure of the entire PS II complex, its own conformation appears to be regulated by the S states of the OEC (31). This reinforces the idea that this protein fine-tunes the water oxidation cycle in some way.

In this paper, we report the results of the use of ESEEM spectroscopy to probe exchangeable hydrogen nuclei at the Mn site in the presence and absence of the 33 kDa protein. ESEEM is a pulsed EPR technique that measures relatively weak magnetic coupling between an electron spin, here the one associated with the S_2-state multiline signal of the Mn cluster, and nuclear spins of nearby ligand atoms out to a distance of ca. 5 Å. Three-pulse ESEEM utilizes a pulse sequence that leads to formation of a “stimulated” spin echo; unlike its two-pulse counterpart, this technique offers the advantage to suppress the modulation effect of an unwanted class of nuclei (32, 33). We also performed a refined EXAFS analysis, using an improved technology compared to that of Cole et al. (28), to detect possible changes of the Mn cluster structure in the absence of the 33 kDa protein. In addition, we used deuterated glycerol to test whether its long-known effect on the EPR signals of the Mn cluster is due to direct binding at the OEC, as is the case for methanol. Both alcohols shift the equilibrium between the two S_2-state signals (multiline and $g = 4.1$ signals) toward the multiline signal (2).

Experimental Procedures

PS II membranes ("BBY" particles) were prepared from spinach as in ref 34. Each independent preparation (four for ESEEM and three for XAS) was split into two aliquots, one for depletion of the 33 kDa protein (along with the 17 and 23 kDa proteins) and one as a control. Depletion of the 33 kDa protein has been performed using the urea (27) or the $CaCl_2$ (28) method. For comparison, an additional sample was depleted for the 17 and 23 kDa proteins only (27). Loading of EPR samples has been performed as in ref 27. For EXAFS analysis, the samples were finally resuspended in 26 mL of the last washing buffer and pelleted at 40.000 rpm for 70 min at 4 °C in a Ti60 rotor. The very dry pellet was loaded into Lucite holders (inner dimensions 18 × 2.5 × 0.8 mm) with a spatula and frozen in liquid nitrogen. All procedures were done in dim green light.

For D_2O experiments, 33 kDa protein-depleted samples were equilibrated with D_2O by washing the pellet, obtained after the second urea or $CaCl_2$ treatment, two times with buffer A/200 mM NaCl made with pure D_2O. Using a glass electrode, this buffer was set to a pH of 5.6, corresponding to a pD of 6.0 (35), with solid NaOH (to minimize the concentration of protons). Undepleted samples were kept on ice during depletion of their counterpart aliquot and were washed two times with buffer A made with D_2O as above. The total time of exposure to D_2O was ca. 1 h until freezing and exactly the same for parallel samples (plus/minus 33 kDa protein) which were to be compared in subsequent analysis. Unlabeled samples were washed two times with the respective buffers made with H_2O.

For glycerol treatments, undepleted and 33 kDa protein-depleted samples, obtained as in ref 27, were finally washed once with buffer A or buffer A/200 mM NaCl, respectively, containing 30% m/v unlabeled glycerol (h_8-glycerol) or an equimolar amount of glycerol deuterated at the nonexchangeable positions (d_5-glycerol, Cambridge Isotope Laboratories Inc.). Samples were repelleted after 30 min of dark incubation on ice.

Oxygen evolution measurements and Western analysis using an anti 33 kDa protein antibody were performed as in ref 27. Continuous wave EPR spectra were measured on a Bruker ECS 106 X-band spectrometer equipped with a Bruker ER4116DM cavity, an Oxford ESR900 liquid helium cryostat, and an Oxford ITC503 temperature controller. Pulsed EPR spectra were measured on a home-built X-band spectrometer (36). First dark-adapted and then illuminated spectra were measured; the analyzed light minus dark difference spectra then show modulation only from nuclei coupled to the light-induced S_2-state multiline signal, and not from any background paramagnetic signals. Illumination was performed at 200 K as in ref 27.

X-ray absorption spectroscopy of dark-adapted samples was performed at the wiggler beamline 7-3 of the Stanford Synchrotron Radiation Laboratory with a beam current of 65–100 mA at 3.0 GeV as detailed in ref 37. The unfocused beam was dispersed by a Si[220] double-crystal monochro-mator, and a 13-element Ge detector measured the Mn X-ray fluorescence, F, which yielded the absorption as F/F_0 (I_0 = incident flux). The sample temperature was maintained at 10 K with a CF1208A cryostat (Oxford Instruments). $KMnO_4$ was used for energy calibration. Scans were collected from 6520 to 7100 eV with step sizes of 0.2 eV in the XANES region (6535–6575 eV) and 0.05 $Å^{-1}$ in the EXAFS region (k = 2–12 $Å^{-1}$). Four XANES and ca. 20 EXAFS scans were averaged. Data were analyzed as in ref 37. Briefly, the K-edge was defined as the zero crossing of the second derivative of the XANES spectrum. For EXAFS, the energy E was converted to the wave vector k:

$$k=(2\pi/h)[2m_e(E-E_0)]^{1/2}$$

where h is Planck's constant, m_e the electron mass, and E_0 the edge peak (6563 eV), weighted by k^3 and background-subtracted. Finally, Fourier transforms were calculated. Details of the EXAFS and fitting methodology are described in the Supporting Information.

Results

Oxygen evolution activities in saturating light were 310–570 (μmol of O_2) h^{-1} (mg of chlorophyll) $^{-1}$ for undepleted and 130–200 (μmol of O_2) h^{-1} (mg of chlorophyll) $^{-1}$ for 33 kDa protein-depleted PS II membranes. Depleted samples showed 35–43% activity compared to untreated aliquots of the same preparation. The reduced activity reflects a slower $S_3 \rightarrow S_0$ state transition (25). At nonsaturating light intensities depleted samples approached ca. 80% of the control; this reflects the fraction of enzymatically active centers. Western blot analysis confirms the complete removal of the 33 kDa protein; Figure 1 shows intact and depleted samples of a representative preparation (preparation 5, used for EXAFS analysis). The depleted sample (lane a) displays a much fainter band than 0.5% of the intact aliquot (lane b).

Representative CW-EPR control spectra (from preparation 6, used for EXAFS analysis) are shown in Figure 2. They display the S_2-state multiline signal at $g = 2$ in the presence (trace a) and absence (trace b) of the 33 kDa protein, with minor modifications in the high-field hyperfine pattern as reported previously (27, 38). A clear $g = 4.1$ signal, seen in the spectrum of the undepleted sample, is missing in the depleted sample, as reported before (27). The substructure of the multiline peaks has been shown to be entirely due to partially resolved hyperfine coupling of the four ^{55}Mn nuclei to the electron spin rather than to “superhyperfine” coupling of ligand nuclei. This has been demonstrated through the lack of differences in the multiline signal after ^{14}N–^{15}N, Cl^-–Br^-, or H_2O–D_2O exchange (2). We repeated this test with PS II samples lacking the 33 kDa protein as a pretest to our pulsed EPR analysis (vide infra), which provides a much more sensitive method to address changes in super-hyperfine couplings. If more D_2O molecules were coupled to the Mn cluster in this case, there might be a contribution of deuteron coupling to the CW multiline substructure. A small field modulation amplitude (0.5 G) was used to increase the sensitivity for small changes in line shape. The comparison of second-derivative multiline spectra of H_2O-versus D_2O-treated samples failed to detect changes in line width or line shape, in the presence or absence of the 33 kDa protein (not shown).

For three-pulse ESEEM analysis of water access to the OEC, four independent preparations of PS II membranes were used; for each an aliquot of the intact sample was compared with a 33 kDa protein-depleted aliquot for which the urea method (preparations 1–3) or the $CaCl_2$ method (preparation 4) was used. Figure 3 shows three-pulse ESEEM traces from dark-adapted (traces a) and illuminated (traces b) undepleted samples that have been equilibrated with D_2O (panel A) or H_2O (panel B), as well as light-minus-dark difference traces (traces c). Modulation of the multiline-specific spin echo by deuterons magnetically coupled to Mn is evident in the difference trace of panel A, whereas the (smaller) proton modulation of panel B is largely suppressed because of proper choice of the τ value; this is important to obtain the pure deuteron modulation after ratioing (vide infra), which eliminates only contributions of nuclei (here ^{14}N) present in both H_2O and D_2O traces. The difference traces have then been normalized to the sample concentration by normalizing at the first maximum of the deuteron modulation; this approximately represents the unmodulated spin-echo intensity which is thus proportional to the spin concentration. This procedure is a good

approximation, if the echo decay is comparable for H_2O and D_2O samples. Spectra of H_2O- and D_2O-treated 33 kDa protein-depleted samples were measured in an analogous way (not shown). A total of 14 of the 16 normalized difference traces (H_2O/ D_2O for plus/minus 33 kDa protein from four independent preparations) aligned well (not shown), demonstrating a fairly reproducible echo decay (essentially spin–spin relaxation). Two traces which deviated by ca. 20% and 60%, respectively, have been rescaled to the average decay (using double-exponential fits). The normalized D_2O and H_2O difference traces have been ratioed to obtain the pure deuteron modulation. Ratioed time domain spectra correspond to difference frequency domain spectra. Figure 4 compares these D/H ratio traces of undepleted and 33 kDa protein-depleted samples from each preparation. For preparation 1 the first maxima are slightly larger than unity because the H_2O trace had a smaller intensity than the D_2O trace at a position (420 ns) immediately before the position of normalization (440 ns). A comparison of the four panels shows some sample-to-sample variation, but no reproducible change of the modulation depth, which reflects the number and/or distance of deuterons coupled to Mn, is evident for 33 kDa protein-depleted samples. The traces of preparation 2 are overlayed with the ratio trace of a D_2O-treated PS II sample lacking the 17 and 23 kDa extrinsic proteins only. All three traces are very similar.

For a quantitative approach we assume that the modulation depth of the first two deuteron cycles is dominated by one (the closest) deuteron. We used the procedure of Mims (39) that had previously been applied to xanthine oxidase (40) to obtain an upper limit for changes in the distances between the deuterons and Mn, and we refer to ref 15 for a more complete analysis. The modulation depth (*d*) was calculated as

$$d = (A+B-2T)/(A+B)$$

where *A* and *B* are the first and second maxima, respectively, and *T* is the first minimum of the ratio trace. This translates into a deuteron–Mn distance, *r* (strictly the distance between the closest deuteron and the center of the electron spin delocalized over the four Mn ions):

$$d = (32/5)(g\beta/\mathbf{H}_0 r^3)^2$$

where *g* is the apparent *g* factor of the excited hole of the multiline signal (calculated from the used microwave frequency *v* as $h\nu/\beta\mathbf{H}_0$), β the Bohr magneton, and $\mathbf{H}_0$ the static magnetic field. This is a good approximation for dipolar coupling where the modulation occurs at the deuteron Larmor frequency (ca. 2 MHz at the static field used in this study), without side peaks in the Fourier transform spectrum (not shown) that would indicate strong exchange coupling. Table 1 shows the results for the four independent PS II preparations. For preparation 1, removal of the 33 kDa protein results in a 1% increase of the apparent D–Mn distance (decrease of modulation), for preparation 3, a 1% decrease of the distance (increase of modulation) was observed, and virtually no change was evident for preparations 2 and 4. Despite this small sample-to-sample variation, we regard these data as evidence that the 33 kDa protein does not influence D_2O binding to the OEC in the S_1 state (illumination at 200 K to advance the samples to the S_2 state largely precludes ligand rearrangements).

In a reciprocal measurement we addressed nonexchangeable protons at the Mn site in a D_2O background. Here we chose τ to maximize the proton modulation. The modulation by exchangeable deuterons is still dominating (Figure 5). Since the ratio technique is not applicable in this case, we compared the small proton peak in the Fourier transform (see the

inset) of the time domain light-minus-dark difference traces obtained from D_2O-treated undepleted and 33 kDa protein-depleted samples after normalization to the first maximum. The peaks, centered at the proton Larmor frequency at the used static field (14.5 MHz), show no difference in intensity or line width.

Figure 2 also shows CW-EPR spectra of undepleted (trace c) and 33 kDa protein-depleted PS II membranes (trace d) after treatment with 30% glycerol. The expected effect on the g = 4.1 signal is seen: it is largely reduced compared to those of samples resuspended in the conventional sucrose buffer (trace a). Interestingly, a clear although also reduced g = 4.1 signal is seen in the 33 kDa protein-depleted sample. This signal cannot be attributed to residual undepleted centers which are present to less than 0.5% (see Figure 1). Figure 6A shows three-pulse ESEEM traces of dark-adapted (trace a) and illuminated (trace b) 33 kDa protein-depleted, d_5-glycerol-treated PS II membranes as well as the light-minus-dark difference trace (trace c and panel B, solid trace a). The low-frequency modulation seen in this difference trace is identical to that of the difference trace of the h_8-glycerol-treated sample (panel B, dotted trace a) and thus cancels in the D/H ratio (trace c). This modulation at ca. 4 MHz arises from nitrogen coupled to Mn (41). An analogous analysis of undepleted samples gave the same result (panel B, trace b). Consequently, there is no detectable coupling of glycerol-derived deuterons to the Mn cluster, irrespective of the presence or absence of the 33 kDa protein. From the noise level we estimate, using the simple modulation depth analysis (vide supra), a minimal distance of 6 Å between glycerol and the Mn cluster. This is clearly incompatible with direct ligation to Mn. We note that at the low-field position of 3220 G appreciably more deuteron modulation was detected (more than expected from the weak field dependence of the modulation depth); we regard the high-field data (3420 G) to be more significant since it is known that the low-field side of g = 2 has more Mn^{2+} contribution to which we attribute the observed modulation difference.

Figure 7 shows the XANES spectra from undepleted and 33 kDa protein-depleted PS II samples in the S_1 state. Each spectrum is the average from three independent PS II preparations. The Mn K-edge positions and shapes are almost identical for the two types of samples. The zero crossing of the second derivative defines the inflection-point energy, an indication of the K-edge position, which is 6552–6553 eV for both traces. The EXAFS k-space spectra (Figure 8) and their Fourier transforms (Figure 9) also show average traces from three independent PS II preparations. Table 1 of the Supporting Information lists the number and distances of backscattering atoms extracted from fits to the spectra from the three individual preparations. No significant changes in the Mn–O/N (∼1.8 Å) and Mn–Mn distances (∼2.7 and ∼3.3 Å) were observed when undepleted and 33 kDa protein-depleted PS II preparations were compared.

Discussion

Three properties of the OEC are modulated by the 33 kDa protein: (i) the structural stability via correct Cl^- binding or via keeping Cl^- in a “sequestered domain”, ii) the kinetics of the slow (late) $S_3 \rightarrow S_0$ state transition (probably via Cl^- binding), (iii) limited access of small molecules. In this paper we address the question of whether the third statement holds for the substrate (water) as well. In principle, limitation of water access could be a thermodynamic or kinetic limitation: in the first scenario, the OEC cleft in the PS II protein would be opened in the absence of the 33 kDa protein so that more water molecules could bind at or near Mn; in the second scenario, the number of water sites at or near Mn would be preserved in the absence of the 33 kDa protein, but the exchange rates into and out of these sites would be elevated, so that the 33 kDa protein merely acts as a diffusion barrier.

From our ESEEM analysis the first case can be ruled out: no increase of proton coupling to Mn and thus no increase of the number of bound H_2O or OH^- species in the first or second coordination sphere of the Mn cluster was observed. It has been proposed that the 33 kDa protein could provide an O-ligand that would be replaced by H_2O or OH^- upon removal (25). This is incompatible with the crystal structure of PS II (7) and also with our results, since we do not find an increase of modulation after removal of this protein. On the other hand, we also fail to see contributions of nonexchangeable hydrogens to the modulation that would decrease after removal of the 33 kDa protein. Thus, our results agree with the general view that the 33 kDa protein does not provide a Mn ligand or outer sphere component. The unchanged modulation depth after 33 kDa protein depletion also indicates that the bonding lengths of the water molecules coordinating Mn are not appreciably altered, reflecting an unchanged OEC structure. A prerequisite for our comparison of spectra from undepleted and 33 kDa protein-depleted PS II is our previous report that the coupling regime within the Mn cluster, as measured with nitrogen ESEEM, is not changed in the absence of the 33 kDa protein (27). A change of the overall coupling could potentially rescale the proton/deuteron contributions in the 33 kDa protein depletion spectra, masking a real change of the number or distances of these nuclei close to Mn.

This ESEEM result is in agreement with our refined XAS results. We present XANES and EXAFS data from PS II samples poised in the S_1 state using a refined XAS methodology with respect to ref 28 (10 versus 150–190 K sample temperature, improved fluorescence detector, newer fitting protocols) which might allow the detection of small long-range structural changes. The K-edge position, which depends on the oxidation states of the four Mn atoms of the cluster, is 6552–6553 eV for both undepleted and 33 kDa protein-depleted PS II, showing that the Mn cluster does not change its redox state upon 33 kDa protein depletion. We interpreted this value as an S_2-state configuration of Mn^{III}-$Mn^{IV}{}_3$ in previous studies (11). The EXAFS analysis revealed the same number and distances of neighboring atoms at ∼1.8 Å (O and/or N atoms) and at ∼2.7 Å (Mn-Mn interaction) for PS II with or without bound 33 kDa protein, in agreement with ref 28 and with numerous studies of intact PS II (11). The third peak which was not detectable in ref 28 is seen at ∼3.3 Å in 33 kDa protein-depleted PS II and in untreated PS II. It represents a second Mn–Mn distance, and a Mn–Ca contribution.

However, we can make these statements only for the dark stable S_1 state in which the samples have been trapped prior to the ESEEM or XAS analysis, since illumination at 200 K (for ESEEM) largely precludes ligand rearrangements (20). For the future it should be interesting to see if this result also holds for the S_2 state by “annealing” the sample at higher temperature after illumination to allow for ligand rearrangements. Also a diffusional control by the 33 kDa protein remains to be tested, since we used long-term equilibration of PS II with D_2O in this study.

If the 33 kDa protein limits water access, this does not seem to be critical in the S_1 state, most likely because (partial) water oxidation does not occur yet in this state. Wydrzynski (12) concludes from substrate exchange data that one substrate is already bound to the OEC in the S_0 state; therefore, it is very likely that this H_2O molecule contributes to the measured hydrogens in our ESEEM study. However, it is possible that water molecules (or exchangeable terminal OH^- ligands or OH^- bridges at/between Mn ions) other than substrate molecules are present at or near Mn. Indeed, from CW-EPR studies of $H_2{}^{17}O$ binding to Mn, Hansson et al. (18) concluded that at least 6 H_2O molecules are present at the Mn site. From a mass spectroscopy study, a reactive pool of 12 H_2O molecules in the OEC was concluded (42). From EPR studies the presence of ligand-deficient Mn in the OEC was postulated (43), and Wydrzynski et al. (29) proposed the binding of nonsubstrate water at such a site. Indeed, the protein-derived Mn ligands modeled into the crystal structure of the

OEC leave a number of coordination sites open to water binding to make each Mn 6-coordinate as expected (7). Of course, all these nonsubstrate ("structural" and "matrix") water molecules, within ca. 5 Å from the Mn ions, would contribute to the measured modulation in the present study.

The 33 kDa protein might control access in higher S-state transitions where it is more critical to limit the number of water molecules at/near the Mn site to avoid side reactions. Such an S-state-dependent fine-tuning of the properties of the 33 kDa protein is indeed likely: first indications are a conformational change upon Mn reduction with hydroxylamine (31) and deprotonation of a carboxylic acid residue upon the S_1–S_2 transition (44). Alternatively or additionally, the 33 kDa protein might regulate proton exit from the OEC to the lumenal phase via an H-bonding network. Such a water entry and/or proton exit channel could be represented by a hydrophilic pathway within this protein detected in the crystal structure (7).

We also report ESEEM data that address glycerol binding to the Mn site in a manner analogous to that for water binding. No deuteron modulation after treatment of either intact or 33 kDa protein-depleted PS II with labeled glycerol was detected. The result clearly rules out direct ligation to Mn. This is surprising since from the similar effect of glycerol and other small alcohols (methanol, ethanol, ethylene glycol) on the $g = 4.1$ signal (see Figure 2) (2) it was assumed that all these compounds would bind to the Mn site, which was explicitly shown for methanol (20). It must be postulated that the mechanisms of $g = 4.1$ signal suppression are different for glycerol and other small alcohols. Glycerol might induce a more global change of the structure of PS II which results in a similar change of the magnetic coupling regime in the Mn cluster. It is worth noting that glycerol has a well-known stabilizing effect on the activity of PS II (see, e.g., ref 45). Interestingly, the lack of Mn binding is not the only difference between glycerol and methanol. Different relaxation effects of these compounds have been reported (46): glycerol decreased the spin relaxation time of the S_2 multiline state, whereas methanol had the opposite effect. Our result is in agreement with Kawamori et al. (47), who concluded from an ENDOR study that glycerol does not bind to the Mn cluster of intact PS II. These authors estimated a cutoff size of ca. 5 Å (between the sizes of ethylene glycol and glycerol) for the access to the Mn site of intact PS II. Finally, our result argues against a model in which glycerol ligates two Mn ions prior to H_2O_2-dependent oxidation to aldehyde (48), unless the centers catalyzing this unusual reaction are structurally perturbed in some way.

Supplementary Material

Refer to Web version on PubMed Central for supplementary material.

References

1. Hankamer B, Barber J, Boekema EJ. Structure and membrane organization of photosystem II in green plants. Annu Rev Plant Physiol Plant Mol Biol. 1997; 48:641–671. [PubMed: 15012277]
2. Debus RJ. The manganese and calcium ions of photosynthetic oxygen evolution. Biochim Biophys Acta. 1992; 1102:269–352. [PubMed: 1390827]
3. Yachandra VK, Sauer K, Klein MP. Manganese cluster in photosynthesis: Where plants oxidize water to dioxygen. Chem Rev. 1996; 96:2927–2950. [PubMed: 11848846]
4. Peloquin JM, Campbell KA, Randall DW, Evanchik MA, Pecoraro VL, Armstrong WH, Britt RD. Mn-55 ENDOR of the S-2-state multiline EPR signal of photosystem II: Implications on the structure of the tetranuclear Mn cluster. J Am Chem Soc. 2000; 122:10926–10942.

5. Zouni A, Witt HT, Kern J, Fromme P, Krauss N, Saenger W, Orth P. Crystal structure of photosystem II from *Synechococcus elongatus* at 3.8 Å resolution. Nature. 2001; 409:739–743. [PubMed: 11217865]
6. Kamiya N, Shen JR. Crystal structure of oxygen-evolving photosystem II from *Thermosynechococcus vulcanus* at 3.7 Å resolution. Proc Natl Acad Sci USA. 2003; 100:98–103. [PubMed: 12518057]
7. Ferreira KN, Iverson TM, Maghlaoui K, Barber J, Iwata S. Architecture of the photosynthetic oxygen-evolving center. Science. 2004; 303:1831–1838. [PubMed: 14764885]
8. Kok B, Forbush B, McGloin M. Cooperation of charges in photosynthetic O_2 evolution-I. A linear four step mechanism. Photochem Photobiol. 1970; 11:457–475. [PubMed: 5456273]
9. Britt, RD. Oxygen evolution. In: Ort, DR.; Yocum, CF., editors. Advances in photosynthesis, oxygenic photosynthesis: the light reactions. Kluwer Academic Publishers; Dordrecht, The Netherlands: 1996. p. 137-164.
10. Hoganson CW, Babcock GT. A metalloradical mechanism for the generation of oxygen from water in photosynthesis. Science. 1997; 277:1953–1956. [PubMed: 9302282]
11. Robblee JH, Cinco RM, Yachandra VK. X-ray spectroscopy-based structure of the Mn cluster and mechanism of photosynthetic oxygen evolution. Biochim Biophys Acta. 2001; 1503:7–23. [PubMed: 11115621]
12. Hillier W, Wydrzynski T. Oxygen ligand exchange at metal sites–simplications for the O_2 evolving mechanism of photosystem II. Biochim Biophys Acta. 2001; 1503:197–209. [PubMed: 11115634]
13. Renger G. Photosynthetic water oxidation to molecular oxygen: apparatus and mechanism. Biochim Biophys Acta. 2001; 1503:210–228. [PubMed: 11115635]
14. Vrettos JS, Limburg J, Brudvig GW. Mechanism of photosynthetic water oxidation: combining biophysical studies of photosystem II with inorganic model chemistry. Biochim Biophys Acta. 2001; 1503:229–245. [PubMed: 11115636]
15. Britt RD, Campbell KA, Peloquin JM, Gilchrist ML, Aznar CP, Dicus MM, Robblee J, Messinger J. Recent pulsed EPR studies of the photosystem II oxygen-evolving complex: implications as to water oxidation mechanisms. Biochim Biophys Acta. 2004; 1655:158–171. [PubMed: 15100028]
16. Weng TC, Hsieh WY, Uffelman ES, Gordon-Wylie SW, Collins TJ, Pecoraro VL, Penner-Hahn JE. XANES evidence against a manganyl species in the S_3 state of the oxygen-evolving complex. J Am Chem Soc. 2004; 126:8070–8071. [PubMed: 15225020]
17. Rutherford AW, Boussac A. Water photolysis in biology. Science. 2004; 303:1782–1784. [PubMed: 15031485]
18. Hansson Ö, Andreasson LE, Vänngard T. Oxygen from water is coordinated to manganese in the S_2 state of photosystem II. FEBS Lett. 1987; 195:151–154.
19. Evans MC, Nugent JH, Ball RJ, Muhiuddin I, Pace RJ. Evidence for a direct manganese–oxygen ligand in water binding to the S_2 state of the photosynthetic water oxidation complex. Biochemistry. 2004; 43:989–994. [PubMed: 14744143]
20. Force DA, Randall DW, Lorigan GA, Clemens KL, Britt RD. ESEEM studies of alcohol binding to the manganese cluster of the oxygen evolving complex of photosystem II. J Am Chem Soc. 1998; 120:13321–13333.
21. Britt RD, Zimmermann JL, Sauer K, Klein MP. Ammonia binds to the catalytic manganese of the oxygen-evolving complex of photosystem II. Evidence by electron spin-echo envelope modulation spectroscopy. J Am Chem Soc. 1989; 111:3522–3532.
22. Messinger J, Nugent JH, Evans MC. Detection of an EPR multiline signal for the S_0* state in photosystem II. Biochemistry. 1997; 36:11055–11060. [PubMed: 9333322]
23. Ahrling KA, Peterson S, Styring S. An oscillating manganese electron paramagnetic resonance signal from the S_0 state of the oxygen evolving complex in photosystem II. Biochemistry. 1997; 36:13148–13152. [PubMed: 9376375]
24. Seidler A. The extrinsic polypeptides of photosystem II. Biochim Biophys Acta. 1996; 1277:35–60. [PubMed: 8950371]
25. Bricker TM, Frankel LK. The structure and function of the 33 kDa extrinsic protein of photosystem II: a critical assessment. Photosynth Res. 1998; 56:157–173.

26. Nield J, Orlova EV, Morris EP, Gowen B, van Heel M, Barber J. 3D map of the plant photosystem II supercomplex obtained by cryoelectron microscopy and single particle analysis. Nat Struct Biol. 2000; 7:44–47. [PubMed: 10625426]
27. Gregor W, Britt RD. Nitrogen ligation to the manganese cluster of photosystem II in the absence of the extrinsic proteins and as a function of pH. Photosynth Res. 2000; 65:175–185. [PubMed: 16228484]
28. Cole JL, Yachandra VK, McDermott AE, Guiles RD, Britt RD, Dexheimer SL, Sauer K, Klein MP. Structure of the manganese complex of photosystem II upon removal of the 33-kilodalton extrinsic protein: an X-ray absorption spectroscopy study. Biochemistry. 1987; 26:5967–5973. [PubMed: 2825768]
29. Wydrzynski T, Hillier W, Messinger J. On the functional significance of substrate accessibility in the photosynthetic water oxidation mechanism. Physiol Plant. 1996; 96:342–350.
30. Boekema EJ, van Breemen JF, van Roon H, Dekker JP. Conformational changes in photosystem II supercomplexes upon removal of extrinsic subunits. Biochemistry. 2000; 39:12907–12915. [PubMed: 11041855]
31. Hong SK, Pawlikowski SA, Van der Meulen KA, Yocum CF. The oxidation state of the photosystem II manganese cluster influences the structure of manganese stabilizing protein. Biochim Biophys Acta. 2001; 1504:262–274. [PubMed: 11245790]
32. Britt, RD. Electron spin echo methods in photosynthesis research. In: Amez, J.; Hoff, AJ., editors. Biophysical techniques in photosynthesis. Kluwer Academic Publishers; Dordrecht, The Netherlands: 1996. p. 235-253.
33. Kevan, L. Modulation of spin-echo decay in solids. In: Kevan, L.; Schwartz, RN., editors. Time domain electron spin resonance. John Wiley and Sons; New York: 1979. p. 279-341.
34. Campbell KA, Gregor W, Pham DP, Peloquin JM, Debus RJ, Britt RD. The 23 and 17 kDa extrinsic proteins of photosystem II modulate the magnetic properties of the S_1-state manganese cluster. Biochemistry. 1998; 37:5039–5045. [PubMed: 9548734]
35. Glasoe PK, Long FA. Use of glass electrodes to measure acidities in deuterium oxide. J Phys Chem. 1960; 64:188–190.
36. Sturgeon BE, Britt RD. Sensitive pulsed EPR spectrometer with an 8–18 GHz frequency range. Rev Sci Instrum. 1992; 63:2187–2192.
37. Cinco RM, Rompel A, Visser H, Aromi G, Christou G, Sauer K, Klein MP, Yachandra VK. Comparison of the manganese cluster in oxygen-evolving photosystem II with distorted cubane manganese compounds through X-ray absorption spectroscopy. Inorg Chem. 1999; 38:5988–5998. [PubMed: 11671305]
38. Seidler A, Rutherford AW. The role of the extrinsic 33 kDa protein in Ca^{2+} binding in photosystem II. Biochemistry. 1996; 35:12104–12110. [PubMed: 8810916]
39. Mims WB, Davis JL, Peisach J. The exchange of hydrogen ions and water molecules near the active site of cytochrome-c. J Magn Reson. 1990; 86:273–292.
40. Lorigan GA, Britt RD, Kim JH, Hille R. Electron spin–echo envelope modulation spectroscopy of the molybdenum center of xanthine oxidase. Biochim Biophys Acta. 1994; 1185:284–294. [PubMed: 8180233]
41. DeRose VJ, Yachandra VK, McDermott AE, Britt RD, Sauer K, Klein MP. Nitrogen ligation to manganese in the photosynthetic oxygen-evolving complex: continuous-wave and pulsed EPR studies of photosystem II particles containing ^{14}N or ^{15}N. Biochemistry. 1991; 30:1335–1341. [PubMed: 1846751]
42. Burda K, Bader KP, Schmid GH. An estimation of the size of the water cluster present at the cleavage site of the water splitting enzyme. FEBS Lett. 2001; 491:81–84. [PubMed: 11226424]
43. Ahrling KA, Pace RJ. Simulation of the S_2 state multiline electron paramagnetic resonance signal of photosystem II: a multifrequency approach. Biophys J. 1995; 68:2081–2090. [PubMed: 7612851]
44. Hutchison RS, Steenhuis JJ, Yocum CF, Razeghifard MR, Barry BA. Deprotonation of the 33-kDa, extrinsic, manganese-stabilizing subunit accompanies photooxidation of manganese in photosystem II. J Biol Chem. 1999; 274:31987–31995. [PubMed: 10542229]

45. Haumann M, Hundelt M, Jahns P, Chroni S, Bogershausen O, Ghanotakis D, Junge W. Proton release from water oxidation by photosystem II: similar stoichiometries are stabilized in thylakoids and PS II core particles by glycerol. FEBS Lett. 1997; 410:243–248. [PubMed: 9237638]

46. Zimmermann JL, Rutherford AW. Electron paramagnetic resonance properties of the S_2 state of the oxygen-evolving complex of photosystem II. Biochemistry. 1986; 25:4609–4615.

47. Kawamori A, Inui T, Ono T, Inoue Y. ENDOR study on the position of hydrogens close to the manganese cluster in S_2 state of photosystem II. FEBS Lett. 1989; 254:219–224.

48. Frasch WD, Mei R, Sanders MA. Oxidation of alcohols catalyzed by the oxygen-evolving complex. Biochemistry. 1988; 27:3715–3719.

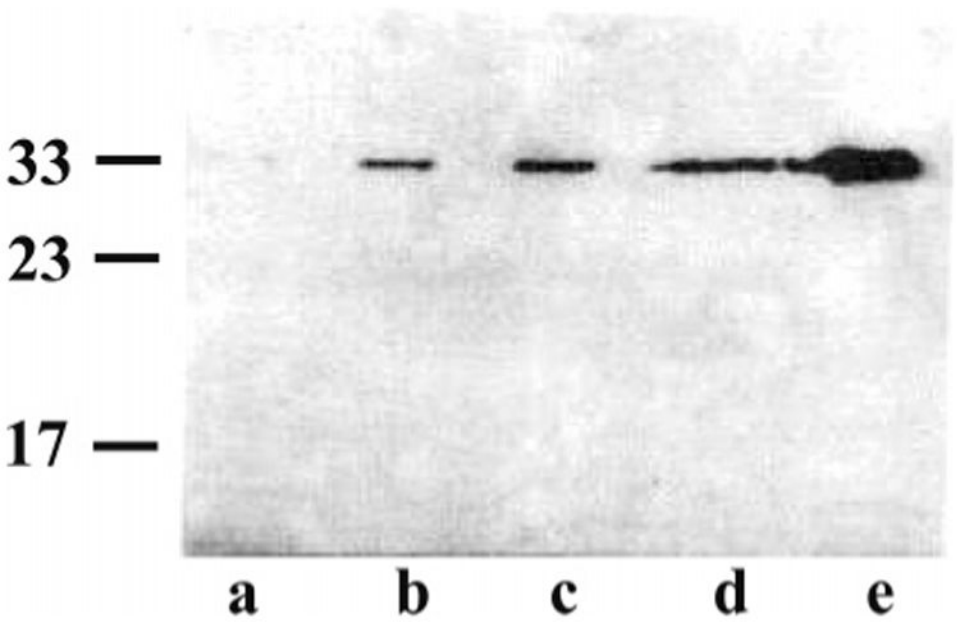

Figure 1.
Western blot of 33 kDa protein-depleted (12 μg of chlorophyll, lane a) and 0.5% (lane b), 1% (lane c), 2% (lane d), and 100% (12 μg of chlorophyll, lane e) untreated PS II membranes.

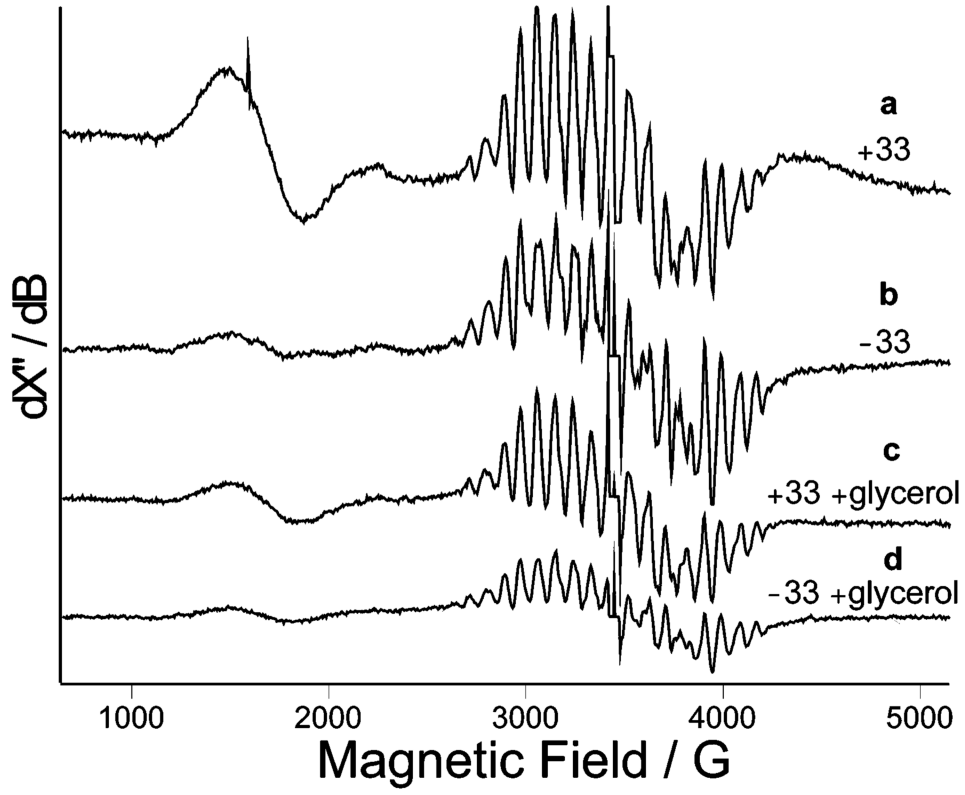

Figure 2.

CW-EPR (light-minus-dark) difference spectra of untreated (a), 33 kDa protein-depleted (b), undepleted/glycerol-treated (c), and 33 kDa protein-depleted/glycerol-treated PS II membranes. The $g = 2$ peak of the stable tyrosine radical Y_D• was deleted from each spectrum. The spectra were normalized to the double-integrated Y_D• signal. Instrumental parameters: microwave frequency, 9.68 GHz; microwave power, 5 mW; field modulation, 10 G/100 kHz; time constant, 41 ms; conversion time, 82 ms; temperature, 7 K; 12–24 scans per trace were averaged.

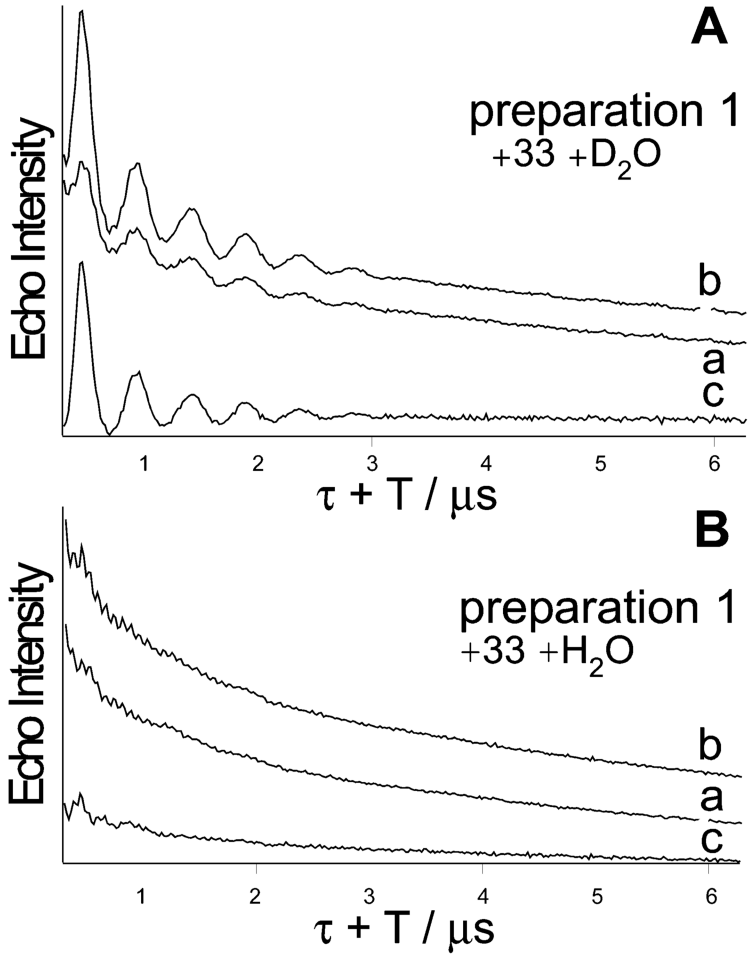

Figure 3.

Time-domain three-pulse ESEEM traces of undepleted PS II membranes from preparation 1 equilibrated with D_2O (panel A) or H_2O (panel B) buffer in the S_1 (traces a) and S_2 (traces b) states. The difference traces (traces c) are trace b minus trace a, respectively. The traces have been offset for clarity. For instrumental parameters, see Figure 4.

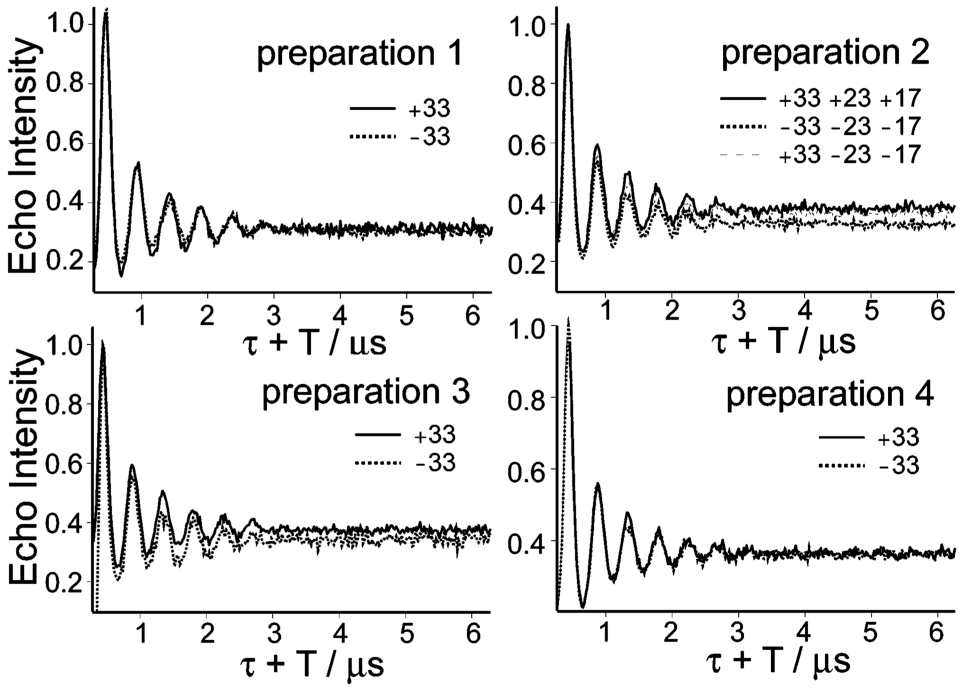

Figure 4.

Three-pulse ESEEM D/H ratio traces of undepleted (solid traces) and 33 kDa protein-depleted (dotted traces) PS II membrane samples from four independent preparations. Each trace is the ratio of normalized difference traces (e.g., Figure 3, traces c) of deuterated and protonated samples. For comparison, the D/H ratio trace of 33 kDa protein-intact, 17/23 kDa protein-depleted PS II membranes is included in the panel “preparation 2” (dashed trace). Instrumental parameters: microwave frequency, 9.265 GHz (preparations 1–3), 9.312 GHz (preparation 4); static field, 3220 G (preparation 1), 3420 G (preparation 2), 3380 G (preparation 3), 3417 G (preparation 4); microwave power, 20.0 W; τ, 219 ns (preparations 1 and 3), 206 ns (preparation 2), 206 ns (preparation 4); T increments, 20 ns; $\pi/2$ pulse, 15 ns; repetition time, 5 ms; temperature, 4 K; each data point is the average of 20 echoes; 40 scans per trace were averaged.

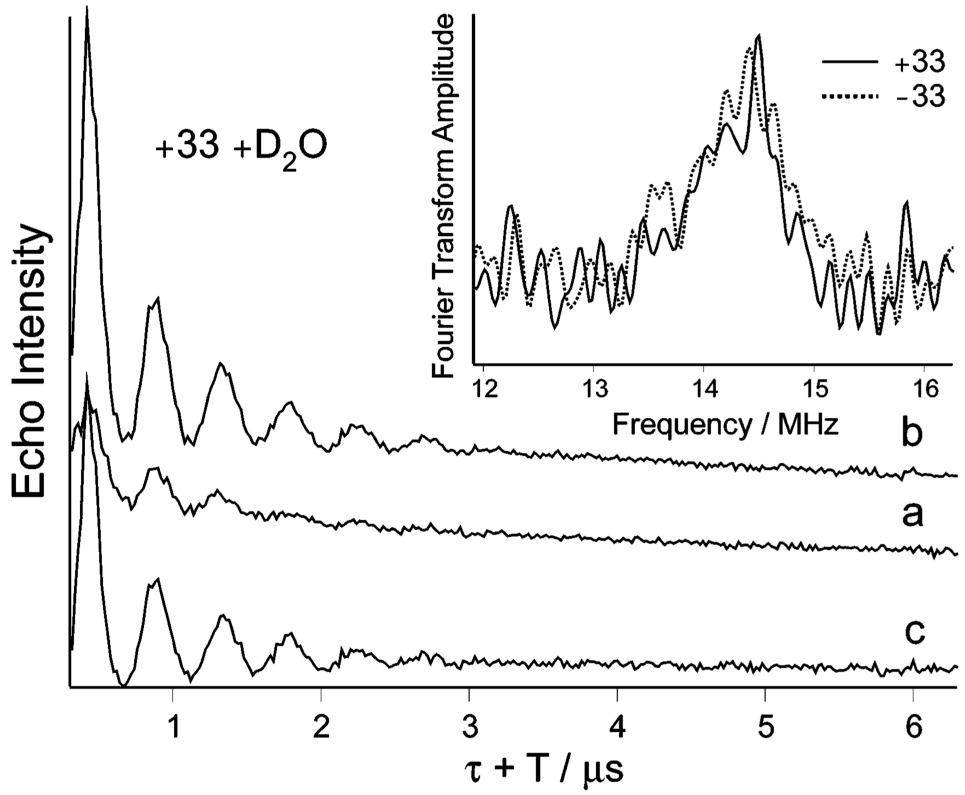

Figure 5.

Time-domain three-pulse ESEEM traces of undepleted PS II membranes in D_2O buffer from preparation 3. Traces a–c and instrumental parameters are as in Figure 4, except a τ value of 238 ns was chosen to maximize ^1H modulation. Inset: Fourier transform spectra of the normalized difference traces (c) of the undepleted (solid trace) and 33 kDa protein-depleted (dotted trace) samples, showing the region around the proton Larmor frequency.

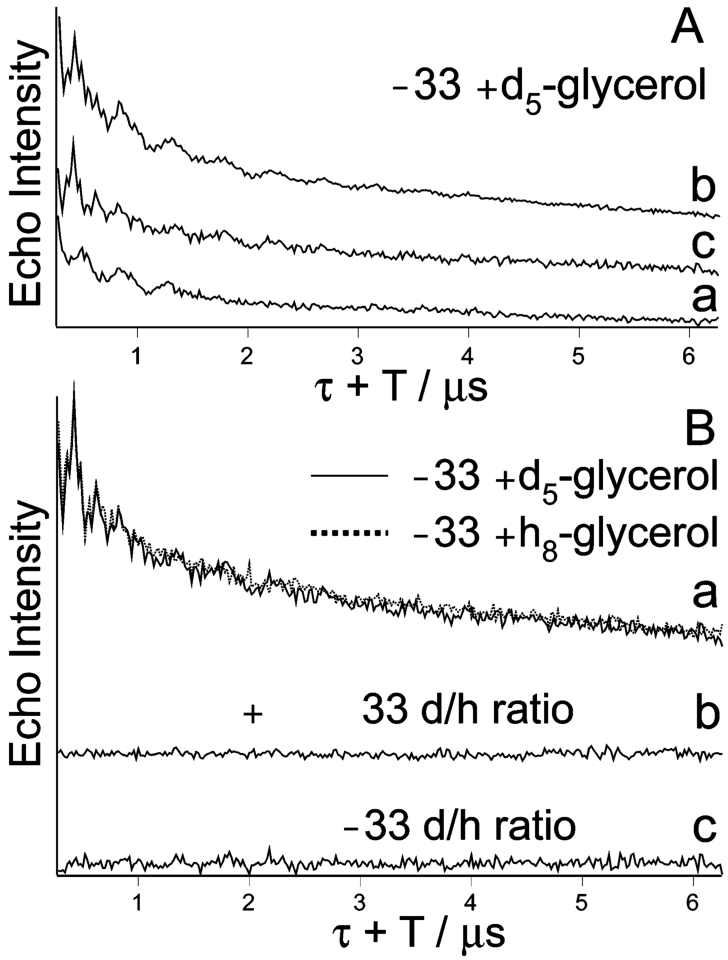

Figure 6.

Time-domain three-pulse ESEEM traces of 33 kDa protein-depleted, d_5-glycerol-treated PS II membranes (panel A) in the S_1 (trace a) and S_2 (trace b) states. The difference trace (trace c) is trace b minus trace a. (Panel B) The difference trace from panel A is shown again (a, solid trace) and overlayed with the corresponding difference trace of the h_8-glycerol-treated sample (a, dotted trace), normalized to each other. The D/H ratio of the two traces is shown in (b). The D/H ratio obtained from undepleted samples in an analogous way is shown in (c). The traces have been offset for clarity. Instrumental parameters are as for preparation 2 (Figure 4).

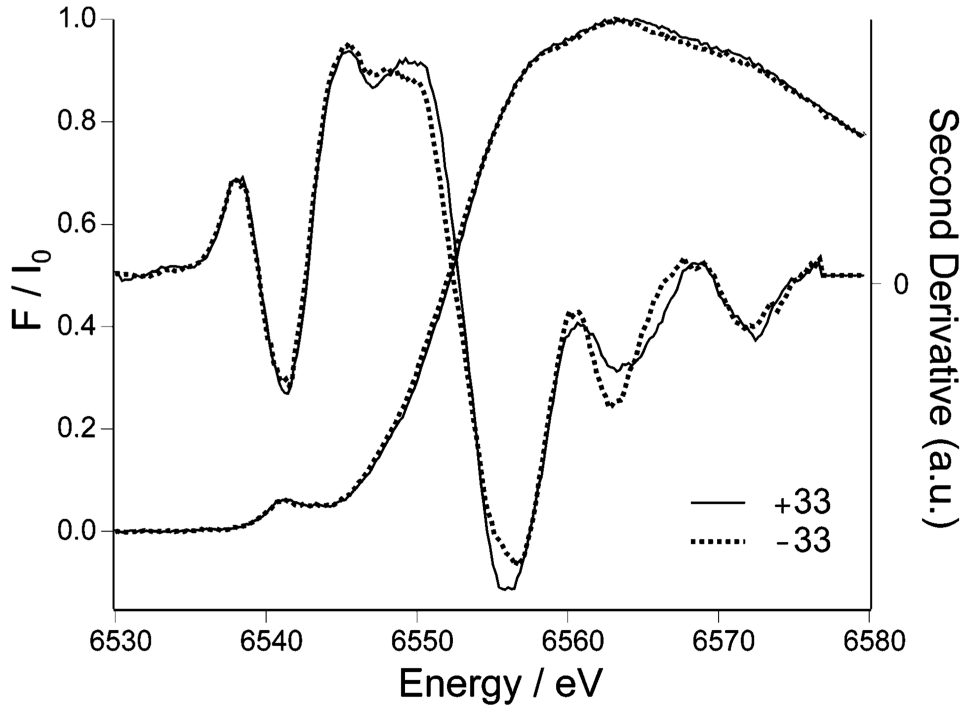

Figure 7.
Normalized Mn K-edge XANES spectra and their second derivatives of untreated (solid trace) and 33 kDa protein-depleted (dotted trace) PS II membranes. Each trace is the average of the spectra from three independent PS II preparations.

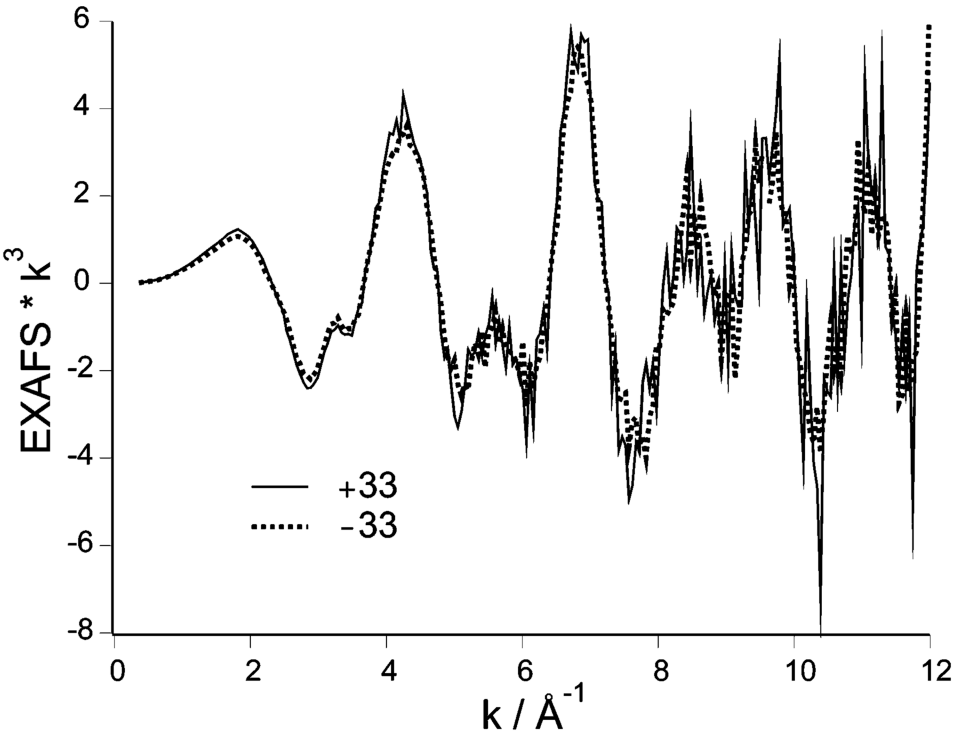

Figure 8.

k^3-weighted EXAFS spectra of untreated (solid trace) and 33 kDa protein-depleted (dotted trace) PS II membranes. Each trace is the average of the spectra from three independent PS II preparations.

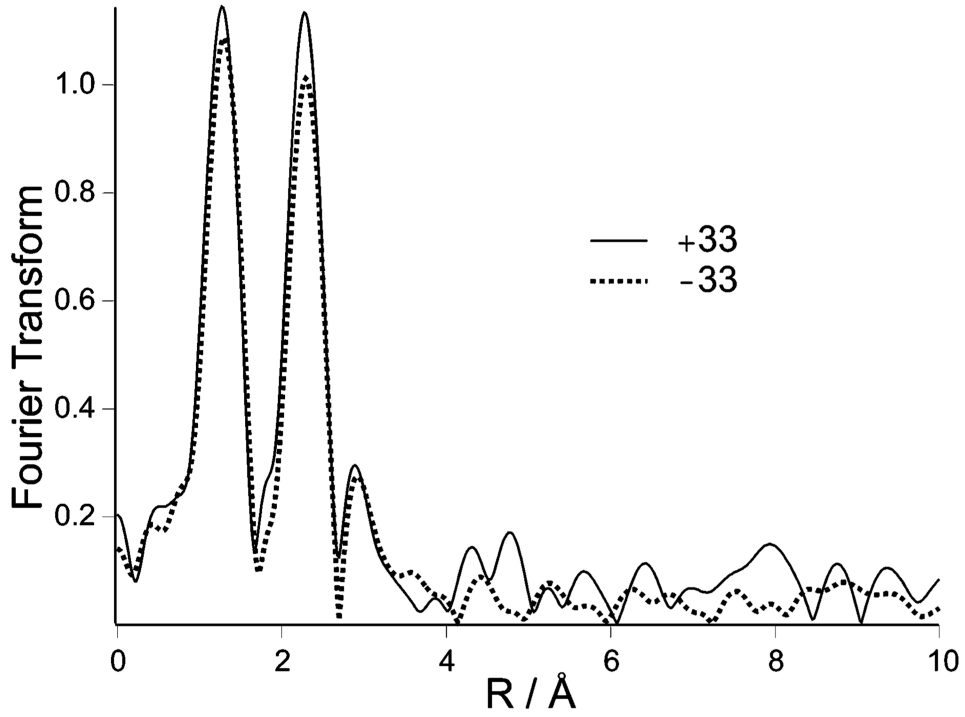

Figure 9.
Fourier transform spectra of EXAFS spectra shown in Figure 8.

Table 1

Deuteron–Mn Distances (*r*/Å) Estimated from the Modulation Depth (*d*, in Parentheses) of Four PS II Preparations

preparation	plus 33 kDa protein	minus 33 kDa protein
1	2.56 (0.797)	2.59 (0.744)
2	2.51 (0.701)	2.50 (0.724)
3	2.55 (0.680)	2.51 (0.733)
4	2.50 (0.726)	2.51 (0.712)